PERGAMON

Chemical Engineering Science 56 (2001) 3197–3210

Chemical Engineering Science

www.elsevier.nl/locate/ces

Reynolds number effects on mixing and reaction in a turbulent pipe flow

Stefan Heinz[a,*], Dirk Roekaerts[b,c]

[a]Technische Universität München, Lehrstuhl für Fluidmechanik, Boltzmannstrasse 15, 85747 Garching, Germany
[b]Department of Applied Physics, Delft University of Technology, Thermal and Fluids Sciences, Lorentzweg 1, 2628 CJ Delft, The Netherlands
[c]Shell Research and Technology Centre, Amsterdam, PO Box 38000, 1030 BN Amsterdam, The Netherlands

Received 3 March 2000; accepted 4 December 2000

Abstract

A new Lagrangian mixing model is presented that describes the turbulent mixing of reacting scalars as a cascade process from large to small scales. The model is derived by applying guidance of Eulerian multi-scale mixing models. Compared to these models, the essential advantage of the derived Lagrangian model is given by the fact that approximations are restricted to the simulation of mixing processes, i.e., chemical transformations are treated exactly. In contrast to previously applied Lagrangian methods for scalar fields, the model presented here is shown to be applicable to inhomogeneous reacting liquid-phase flows. This is of relevance to important practical applications and further developments of models for the scalar mixing in multi-phase flows. Evidence for the derived mixing model in its general formulation is provided for different flows through its full consistency with well-tested Eulerian transport equations. Applications to different homogeneous flows reveal essential features of the mixing model. Two new theoretical findings are presented: First, the appearance of scalar gradients may lead to a significant reduction of the composition frequency. Second, the model structure presented here permits the derivation of an algebraic model for the composition frequency by relatively weak assumptions. The good performance of that algebraic version of the general mixing model is demonstrated by simulating mixing and parallel chemical reactions in a turbulent pipe flow. It is shown that the error of conventional techniques that neglect Reynolds number effects may amount to 50% for the considered case. These errors may be larger if more complex reaction mechanisms have to be considered.

Keywords: Turbulence; Multiphase flow; Mixing; Reaction; PDF method; Multi-scale model

1. Introduction

The calculation of turbulent reacting flows by probability density function (PDF) methods offers significant advantages compared to the application of Reynolds-averaged equation methods, because essential closure problems do not appear that have to be handled in those approaches. Importantly, turbulence–chemistry interactions can be calculated in the PDF approach without having to make assumptions on chemical conversions, i.e., approximations are restricted to the description of turbulent mixing (Pope, 1985, 2000; Fox, 1996; Baldyga & Bourne, 1999). Nevertheless, the simulation of these mixing processes represents an intricate problem: they take place at various scales and their intensity may vary over orders of magnitude. The energy-containing and inertial subranges (see Fig. 1), where mixing is driven through inhomogeneities of mean fields (Pope & Chen, 1990; Pope, 1991; Van Slooten, Jayesh, & Pope, 1998; Heinz, 1998), usually present the most important parts of the spectrum of mixing processes. The consideration of mixing processes at the Kolmogorov and Batchelor scales is often restricted to the modelling of their dissipative influence on the large scales, but their explicit resolution may also be essential for both velocity and scalar fields.

With reference to flow fields, the simulation of mixing processes at the Kolmogorov-scale is especially important near solid walls, where the viscous transport dominates the balance of the turbulent kinetic energy (TKE). Different approaches had been presented to consider these Reynolds number effects in PDF methods. The consideration of the motion of fluid particles leads to

* Corresponding author. Tel.: + 49-(0)-89-289-16146; fax: + 49-(0)-89-289-16139.
E-mail address: heinz@flm.mw.tum.de (S. Heinz).

0009-2509/01/$ - see front matter
PII: S0009-2509(00)00539-X

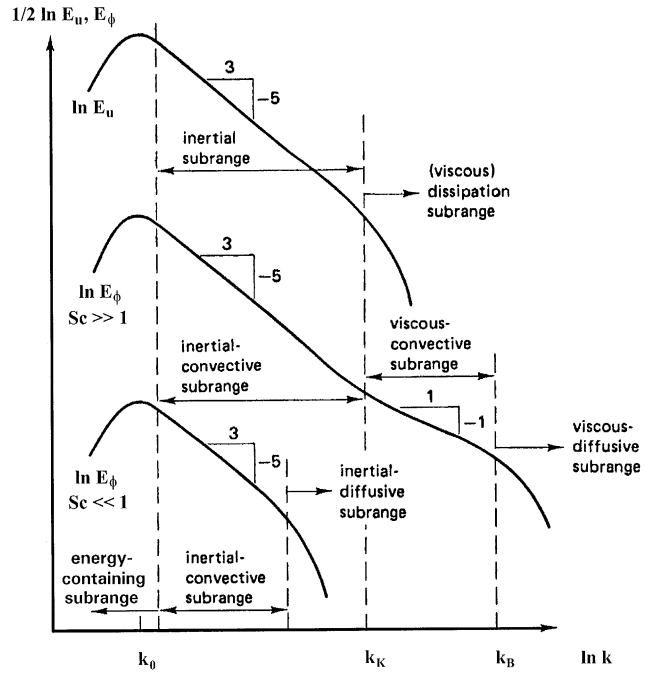

Fig. 1. Idealized energy spectra in fully developed homogeneous, isotropic turbulence as described by Tennekes and Lumley (1972). The velocity spectrum (spectral density function E_u) has a large inertial subrange in between the energy-containing and (viscous) dissipation subrange. The integral-scale (k_0) and Kolmogorov-scale (k_K) wavenumbers are separated through the turbulent Reynolds number $Re_1, k_K = Re_1^{3/2} k_0$. The scalar spectrum (spectral density function E_Φ) has for Schmidt numbers $Sc > 1$ in addition to the inertial-convective a viscous-convective subrange. The Kolmogorov-scale and Batchelor-scale (k_B) wavenumbers are separated through the Schmidt number $Sc, k_B = Sc^{1/2} k_K$. The slopes $-5/3$ and -1 denote the scaling laws $E_u(k) \sim k^{-5/3}, E_\Phi(k) \sim k^{-5/3}$ and $E_\Phi(k) \sim k^{-1}$ in the corresponding subranges.

complicated non-Markovian stochastic equations for particle velocities, because the finite correlation of their accelerations has to be taken into account (Sawford, 1991; Heinz, 1997). These problems can be avoided by considering the motion of stochastic particles (Dreeben & Pope, 1997a, 1998). Such particles undergo both convective motion through the velocity field (as fluid particles) and molecular motion, i.e., the increments of the particle position depend on the velocity field and the kinematic viscosity. A simpler method to take the effect of a wall into account consists in the reflection of its influence through adopting suited conditions near boundaries (Dreeben & Pope, 1997b), which corresponds with the application of wall-functions in Reynolds-stress closure models.

With reference to scalar fields, mixing processes at the Kolmogorov and Batchelor scales are especially important for high-Schmidt number (Sc) reacting flows (liquids). Fig. 1 shows that the Kolmogorov-scale wavenumber k_K and the Batchelor-scale wavenumber $k_B = Sc^{1/2} k_K$ are well separated in that case, i.e., the characteristic transport time from the smallest to the largest wavenumbers is significantly larger than for small-Sc flows (gases) so that there is a remarkable delay of the onset of chemical conversion processes. In dependence on the reaction scheme, this fact may lead to phenomena that are more difficult to predict than the influence of Kolmogorov-scale processes on the structure of velocity fields. That is relevant to many applications in the chemical process industry, where high-Sc flows often appear.

By adopting concepts developed within the Eulerian framework (Fox, 1995), the consideration of Reynolds number effects in Lagrangian simulations of the evolution of scalar fields has been considered previously by Fox (1997, 1999). From a methodological point of view, this approach represents a substantial progress due to its systematic nature of describing the transport of scalar energy as a cascade process from large to small scales. Fox's Lagrangian spectral relaxation (LSR) model describes the multi-scale transport of scalars in gases in a very good agreement with direct numerical simulation (DNS) data. However, comparisons of predictions of the LSR model with DNS or experimental data are not available for Schmidt numbers Sc greater than unity (Fox, 1997), i.e., the model is not tested for that case.

The present paper addresses in particular for high-Schmidt number flows ($Sc \gg 1$) the question, in which way mixing processes at the Kolmogorov and Batchelor scale can be taken into account in Lagrangian PDF methods. The approach is developed by adopting guidance of the Eulerian mixing model of Baldyga to construct the Lagrangian equations (Baldyga & Bourne, 1984a–c, 1988, 1989, 1999; Baldyga, 1989). This model differs considerably from that of Fox: it applies as parameters only three characteristic times related to the mixing at different stages of the spectrum, and it is based on scaling arguments so that no assumptions are required on the shape of spectral functions. Baldyga's model is applicable to the description of the mixing of different scalars in inhomogeneous and instationary flows, and proved for a variety of problems (Baldyga, 1994; Baldyga & Henczka, 1995, 1997; Kruis & Falk, 1996; Baldyga & Bourne, 1999).

The paper is organized as follows. In Section 2, Lagrangian models for the flow field and scalar transport and reaction are presented in order to provide a frame for the model development. In Section 3, the new mixing model is derived by the constraint that the Lagrangian stochastic composition model has to satisfy the Eulerian transport equations of Baldyga's turbulent mixer model. Essential features of that multi-scale mixing model are discussed for homogeneous flows: decaying turbulence and turbulence with local equilibrium are investigated. The performance of a simple algebraic version of this mixing model is illustrated in Section 4, where simulations of mixing and parallel chemical reactions of species in a turbulent pipe flow are compared to measurements.

Finally, the scope of the presented methodology and the differences to other methods are summarized.

2. Lagrangian flow and composition models

In Section 2.1, simple Lagrangian stochastic models for the velocity and mass fractions of species are considered. These models provide a suited frame for the following developments, and they are convenient for the applications considered in Section 4. But in fact, the methodology presented here can also be applied in conjunction with other Lagrangian models (Pope, 1994a; Fox, 1996; Wouters, Peeters, & Roekaerts, 1996). In Section 2.2, Eulerian transport equations for the means and variances of the velocity-composition fields are derived from the Lagrangian models presented in Section 2.1. These budget equations reveal the relationship to usually applied Reynolds-averaged equations and provide the basis for the estimation of the composition frequency in Section 3.

2.1. Lagrangian stochastic models

The simplified Langevin model represents the most simple way of representing Eulerian transport equations in terms of a Lagrangian stochastic model (Pope, 1985, 1994a). It describes the change in time t of positions $\mathbf{x}^* = (x_1^*, x_2^*, x_3^*)$ and velocities $\mathbf{U}^* = (U_1^*, U_2^*, U_3^*)$ of a fluid particle moving with the flow by ($i = 1, 2, 3$)

$$\frac{\mathrm{d}}{\mathrm{d}t} x_i^*(t) = U_i^*, \tag{1a}$$

$$\frac{\mathrm{d}}{\mathrm{d}t} U_i^*(t) = -\rho^{-1}\frac{\partial p}{\partial x_i} - \frac{1}{\tau}\left(\frac{3}{4}C_0 + \frac{1}{2}\right)(U_i^* - \langle U_i\rangle) + \sqrt{C_0\frac{q^2}{2\tau}}\frac{\mathrm{d}W_i}{\mathrm{d}t}. \tag{1b}$$

Here, p is the Reynolds-averaged pressure, ρ the averaged fluid density, $q^2 = \langle u_i u_i\rangle$ twice the TKE and $\tau = q^2/(2\varepsilon)$ the dissipation time scale of turbulence, where ε is the mean dissipation rate of TKE. Eulerian velocity fluctuations are denoted by $u_i = U_i - \langle U_i\rangle$, and summation is assumed for repeated subscripts. The Reynolds-averaged Eulerian velocity $\langle\mathbf{U}\rangle(\mathbf{x}^*, t)$ is written without a star in contrast to Lagrangian quantities. The last term in Eq. (1b) describes the influence of random accelerations. This term is characterized by the white noise $\mathrm{d}W_i/\mathrm{d}t$, which is a Gaussian process with vanishing mean values, $\langle \mathrm{d}W_i/\mathrm{d}t\rangle = 0$, and with uncorrelated values at different times, $\langle \mathrm{d}W_i/\mathrm{d}t(t)\mathrm{d}W_j/\mathrm{d}t'(t')\rangle = \delta_{ij}\delta(t - t')$. The symbol δ_{ij} is the Kronecker delta and $\delta(t - t')$ the delta function. For the parameter C_0 we apply $C_0 = 3.5$ (Dreeben & Pope, 1997b; Heinz, 1998).

Further, we use the often applied 'interaction by exchange with the mean' (IEM) model to simulate the mixing of species. In accord with the treatment of the velocity field, no attempt is made to include molecular transport explicitly (Dreeben & Pope, 1997a, 1998; Colucci, Jaberi, Givi, & Pope, 1998). This approach is justified for the applications considered below and keeps the development of the methodology simple. For other applications involving simulation of the scalar distribution near walls, the consideration of these effects could be essential. The micromixing of the mass fraction Φ_α^* of a scalar α is described by the IEM model as (Pope, 1985)

$$\frac{\mathrm{d}}{\mathrm{d}t}\Phi_\alpha^*(t) = -G_\alpha(\Phi_\alpha^* - \langle\Phi_\alpha\rangle) + \rho^{-1}r_\alpha, \tag{1c}$$

where G_α is an unknown coefficient, which is often modelled by $G_\alpha = C_\varphi/(2\tau)$, i.e. the composition frequency G_α is taken proportional to the turbulence frequency τ^{-1}. C_φ is a constant with a standard value $C_\varphi = 2.0$ (Pope, 1985). The first term on the right-hand side of Eq. (1c) models the scalar micromixing in a formal correspondence to that of momentum in Eq. (1b). The second term $\rho^{-1}r_\alpha(\Phi^*)$ describes chemical transformations exactly, where the fluid density ρ is assumed to be constant for simplicity. In contrast to subscripts i, j, k applied above, no summation convention is used for repeated greek subscripts.

2.2. Relationship to Reynolds-averaged equations

The Eqs. (1a)–(1c) can be transformed into a Fokker–Planck equation for the one-point velocity-composition PDF. From that equation, transport equations can be derived for all moments of this PDF by multiplication with the corresponding variables and integration (Gardiner, 1983; Risken, 1984). By invoking the incompressibility constraint $\partial U_k/\partial x_k = 0$ and the definition of the concentration $C_\alpha = \Phi_\alpha\rho$ of a scalar, these equations read for the mean velocity and concentration

$$\frac{\partial\langle U_i\rangle}{\partial t} + \langle U_j\rangle\frac{\partial\langle U_i\rangle}{\partial x_j} + \frac{\partial\langle u_i u_j\rangle}{\partial x_j} = -\rho^{-1}\frac{\partial p}{\partial x_i}, \tag{2a}$$

$$\frac{\partial\langle C_\alpha\rangle}{\partial t} + \langle U_j\rangle\frac{\partial\langle C_\alpha\rangle}{\partial x_j} + \frac{\partial\langle u_j c_\alpha\rangle}{\partial x_j} = \langle r_\alpha\rangle. \tag{2b}$$

These relations correspond to the exact Reynolds-averaged equations if the acceleration due to gravity and molecular transport terms are neglected. In the same way, budget equations for the variances of the velocity-composition fields can be derived from the Eqs. (1a)–(1c),

$$\frac{\partial\langle u_i u_j\rangle}{\partial t} + \langle U_k\rangle\frac{\partial\langle u_i u_j\rangle}{\partial x_k} + \frac{\partial\langle u_k u_i u_j\rangle}{\partial x_k} + \langle u_k u_i\rangle\frac{\partial\langle U_j\rangle}{\partial x_k} + \langle u_k u_j\rangle\frac{\partial\langle U_i\rangle}{\partial x_k} = -\frac{1}{\tau}\left(\frac{3}{2}C_0 + 1\right)\langle u_i u_j\rangle + C_0\frac{q^2}{2\tau}\delta_{ij}, \tag{3a}$$

$$\frac{\partial\langle u_i c_\alpha\rangle}{\partial t} + \langle U_k\rangle\frac{\partial\langle u_i c_\alpha\rangle}{\partial x_k} + \frac{\partial\langle u_k u_i c_\alpha\rangle}{\partial x_k} + \langle u_k u_i\rangle\frac{\partial\langle C_\alpha\rangle}{\partial x_k} + \langle u_k c_\alpha\rangle\frac{\partial\langle U_i\rangle}{\partial x_k} = -\frac{1}{\tau}\left(\frac{3}{4}C_0 + \frac{1}{2}\right)\langle u_i c_\alpha\rangle - G_\alpha\langle u_i c_\alpha\rangle + \langle u_i r_\alpha\rangle, \quad (3b)$$

$$\frac{\partial\sigma_\alpha^2}{\partial t} + \langle U_k\rangle\frac{\partial\sigma_\alpha^2}{\partial x_k} + \frac{\partial\langle u_k c_\alpha^2\rangle}{\partial x_k} + 2\langle u_k c_\alpha\rangle\frac{\partial\langle C_\alpha\rangle}{\partial x_k} = -2G_\alpha\sigma_\alpha^2 + 2\langle c_\alpha r_\alpha\rangle, \quad (3c)$$

where $c_\alpha = C_\alpha - \langle C_\alpha\rangle$ denotes Eulerian concentration fluctuations and the composition variance $\sigma_\alpha^2 = \langle c_\alpha^2\rangle$ is introduced to simplify the notation applied below.

Eq. (3a) represents a model for the turbulent transport of momentum, which, adopting Kolmogorov's (1942) theory for the dissipation, is fully consistent with Rotta's (1951) turbulence model. A corresponding comparison between the σ_α^2-transport equation derived from the Lagrangian equation (1c) and equations derived within the Eulerian framework is considered in Section 3. This is done, in particular, to estimate the unknown coefficient G_α in Eq. (1c) in terms of the characteristic quantities of the inertial-convective, viscous-convective and viscous-diffusive subranges: τ, the Kolmogorov time scale τ_η and the Schmidt number Sc. Provided that these quantities and boundary and initial conditions are given (see Section 4), Eqs. (1a)–(1c) appear in a closed form because the Eulerian mean velocities, compositions, the mean pressure gradient and the TKE can be evaluated from particle properties: kernel estimates provide weighted means of properties of particles in the vicinity of a point considered, see Pope (1985, 2000) for details.

3. Lagrangian multi-scale mixing model

In Section 3.1, the multi-scale turbulent mixer model of Baldyga (1989) is presented. This model is used in Section 3.2 to estimate the coefficient G_α in Eq. (1c) through the constraint of consistency between the composition covariance transport equation (3c) and Baldyga's model. The composition frequency G_α is provided in that way by means of a system of partial differential equations. In Section 3.3, an algebraic version of that general model is derived, which is of special relevance to practical applications. That model is discussed in Section 3.4: homogeneous, decaying turbulence and turbulence with local equilibrium are investigated.

3.1. Eulerian multi-scale turbulent mixer model

A typical multi-scale micromixing model follows, in a Lagrangian frame, a lump of fluid that mixes with its environment by the following serial steps (Fox, 1996):

(1) Reduction in size down to the Kolmogorov scale, with no change in reactant concentrations, at a rate dependent on the initial fluid particle size relative to the Kolmogorov scale.
(2) Further reduction in size down to the Batchelor scale, with negligible change in reactant concentrations, at a rate proportional to τ_η^{-1}, and
(3) Molecular diffusion and reaction in Batchelor-scale lamellar structures.

The model of Baldyga (1989) reflects these serial steps in a simple way, where only a few parameters are applied. The covariance σ_α^2 of a non-reacting scalar is considered as superposition of three parts: $\sigma_\alpha^2 = \sigma_{\alpha1}^2 + \sigma_{\alpha2}^2 + \sigma_{\alpha3}^2$. These three contributions to σ_α^2 represent the integrals of the spectral scalar density function (see Fig. 1) in the energy-containing and inertial-convective subrange ($\sigma_{\alpha1}^2$), the viscous-convective subrange ($\sigma_{\alpha2}^2$) and the viscous-diffusive subrange ($\sigma_{\alpha3}^2$) of the scalar spectrum. They satisfy the transport equations

$$\frac{\partial\sigma_{\alpha1}^2}{\partial t} + \langle U_j\rangle\frac{\partial\sigma_{\alpha1}^2}{\partial x_j} - \frac{\partial}{\partial x_j}\left[D_T\frac{\partial\sigma_{\alpha1}^2}{\partial x_j}\right] + 2\langle u_j c_\alpha\rangle\frac{\partial\langle C_\alpha\rangle}{\partial x_j} = -\frac{C_\varphi}{\tau}\sigma_{\alpha1}^2, \quad (4a)$$

$$\frac{\partial\sigma_{\alpha2}^2}{\partial t} + \langle U_j\rangle\frac{\partial\sigma_{\alpha2}^2}{\partial x_j} - \frac{\partial}{\partial x_j}\left[D_T\frac{\partial\sigma_{\alpha2}^2}{\partial x_j}\right] = \frac{C_\varphi}{\tau}\sigma_{\alpha1}^2 - E\sigma_{\alpha2}^2, \quad (4b)$$

$$\frac{\partial\sigma_{\alpha3}^2}{\partial t} + \langle U_j\rangle\frac{\partial\sigma_{\alpha3}^2}{\partial x_j} - \frac{\partial}{\partial x_j}\left[D_T\frac{\partial\sigma_{\alpha3}^2}{\partial x_j}\right] = E\sigma_{\alpha2}^2 - G\sigma_{\alpha3}^2, \quad (4c)$$

where $C_\varphi = 2.0$, $E = 0.058/\tau_\eta$ and $G = (0.303 + 17050/Sc)E$. The Schmidt number is defined by $Sc = \nu/D_m$, where D_m is the molecular diffusivity and ν the kinematic viscosity, and the Kolmogorov time scale by $\tau_\eta = (\nu/\varepsilon)^{1/2}$. In general, one has to consider the sum of the molecular and turbulent diffusivity, $D_m + D_T$, instead of D_T, but D_m is neglected here for simplicity, which is justified for the applications considered below.

The description of viscous-convective and -diffusive mixing processes through Eqs. (4a)–(4c) is adequate when the turbulent Reynolds number $Re_1 = \tau/\tau_\eta$ and the Schmidt number Sc fall in a certain range. These two non-dimensional parameters determine the ratios of E to C_φ/τ and G to E: $E\tau/C_\varphi = 0.029Re_1$ and $G/E = (0.303 + 17050/Sc)$. The first condition for the validity of Eqs. (4a)–(4c) is $Re_1 \geqslant 11.6$, or, $Re_\lambda \geqslant 30$ in terms of the Taylor-scale Reynolds number $Re_\lambda = 2.582Re_1$ (Baldyga, 1999). This constraint ensures that the Kolmogorov and Obukhov–Corrsin constants, which are applied to the estimation of the constants which appear

in Eqs. (4a)–(4c), can be considered as practically constant, i.e., as independent of Re_λ (Sreenivasan, 1996). The second condition for the validity of Baldyga's model (Eqs. (4a)–(4c)) is a large Schmidt number, $Sc \gg 1$ (liquids), so that a well-developed viscous-convective subrange exists, see Fig. 1.

In the preparation of the comparison with the σ_α^2-transport equation (3c), we derive a formally closed equation for σ_α^2 by taking the sum of Eqs. (4a)–(4c),

$$\frac{\partial \sigma_\alpha^2}{\partial t} + \langle U_j \rangle \frac{\partial \sigma_\alpha^2}{\partial x_j} + \frac{\partial \langle u_j c_\alpha^2 \rangle}{\partial x_j} + 2\langle u_j c_\alpha \rangle \frac{\partial \langle C_\alpha \rangle}{\partial x_j} = -GS_{\alpha 3}\sigma_\alpha^2, \tag{5a}$$

where $S_{\alpha 3} = \sigma_{\alpha 3}^2/\sigma_\alpha^2$ is introduced and the definition of D_T through $D_T\, \partial \sigma_\alpha^2/\partial x_j = -\langle u_j c_\alpha^2 \rangle$ is applied. Relation (5a) reveals that molecular diffusion is the only mechanism of mixing on the molecular scale. However, the mixing frequency $GS_{\alpha 3}$ depends strongly on the rates of inertial and viscous convective mixing. It can be proved by Eqs. (4a)–(4c) that $S_{\alpha 3}$ satisfies the equation system

$$\frac{\partial S_{\alpha 3}}{\partial t} + \left[\langle U_j \rangle - 2\frac{D_T}{\sigma_\alpha^2}\frac{\partial \sigma_\alpha^2}{\partial x_j} \right] \frac{\partial S_{\alpha 3}}{\partial x_j} - \frac{\partial}{\partial x_j}\left[D_T \frac{\partial S_{\alpha 3}}{\partial x_j} \right] = ES_{\alpha 2} + S_{\alpha 3}[GS_{\alpha 3} - \gamma_\alpha - G], \tag{5b}$$

$$\frac{\partial S_{\alpha 2}}{\partial t} + \left[\langle U_j \rangle - 2\frac{D_T}{\sigma_\alpha^2}\frac{\partial \sigma_\alpha^2}{\partial x_j} \right] \frac{\partial S_{\alpha 2}}{\partial x_j} - \frac{\partial}{\partial x_j}\left[D_T \frac{\partial S_{\alpha 2}}{\partial x_j} \right] = S_{\alpha 2}\left[GS_{\alpha 3} - \gamma_\alpha - E - \frac{C_\varphi}{\tau} \right] + \frac{C_\varphi}{\tau}(1 - S_{\alpha 3}). \tag{5c}$$

Here, the abbreviations $S_{\alpha 2} = \sigma_{\alpha 2}^2/\sigma_\alpha^2$ and $\gamma_\alpha = -2\langle u_j c_\alpha \rangle (\partial \langle C_\alpha \rangle/\partial x_j)/\sigma_\alpha^2$ are introduced. By adopting algebraic expressions for $\langle u_j c_\alpha \rangle$ and $\langle u_i u_j \rangle$ according to Eqs. (3a)–(3b) with $r_\alpha = 0$, the expression γ_α related to the scalar gradient can be simplified to $\gamma_\alpha = \lambda\tau(q^2/\sigma_\alpha^2)[\partial \langle C_\alpha \rangle/\partial x_j]^2$, where $\lambda = 8C_0/[(3C_0 + 2)(3C_0 + 2 + 4G_\alpha\tau)]$.

It is worth noting that the Eulerian model (Eqs. (5a)–(5c)), which is used in Section 3.2 for the derivation of the Lagrangian multi-scale mixing model, differs from the spectral relaxation (SR) model, which was used by Fox as guideline for the construction of his LSR model (Fox, 1995, 1997). Due to the reference to the Kolmogorov and Obukhov–Corrsin constants, the allowed Re_1-range is approximately the same in both models (the SR model is applicable if $Re_1 \geqslant 8$, or, $Re_\lambda \geqslant 20.7$), but the model of Fox may be applied to both small- and large-Sc flows. The concept to construct a multi-scale mixing model for both gases and liquids is attractive, but, in contrast to Baldyga's model, comparisons of the predictions of Fox's model with experimental results for large-Sc flows are presently not available. The assessment of mixing models for such flows through DNS appears to become feasible, but presently, suited DNS data do not exist. A significant progress has been achieved recently by Chasnov (1998), who performed DNS of flows with Sc-variations between $1 \leqslant Sc \leqslant 10^3$. The turbulent Reynolds number varied in these simulations between $12.5 \leqslant Re_1 \leqslant 32.5$. These DNS data reveal that there is a remarkable effect of Sc on the mixing. However, the present computer resources limit these DNS calculations to two-dimensional flows and do not allow the resolution of the scalar spectrum for $Sc \geqslant 20$ in such a way that the characteristic mixing time could be derived properly.

3.2. Multi-scale Lagrangian mixing model

The comparison of the composition covariance transport equation (3c) derived from the Lagrangian model and Baldyga's equation (5a) for a non-reacting scalar ($r_\alpha = 0$) reveals that both equations are identical provided that

$$G_\alpha = 0.5GS_{\alpha 3}. \tag{6}$$

Combined with suited initial and boundary conditions, the Lagrangian equation (1c) in conjunction with Eqs. (6) and (5b)–(5c) represents our Lagrangian multi-scale mixing model. With reference to its IEM-structure, we denote it as multi-scale interaction by exchange with the mean (MSIEM) model. We note that this generalization of the IEM model is essentially different from the generalized IEM model introduced by Tsai and Fox (1995). The latter model relates the composition frequency to the change of a shadow scalar field, which is not determined through the model and has to be provided as an input. In contrast to that, the MSIEM model calculates the composition frequency in dependence on the characteristic mixing times of the processes involved.

According to Pope (1983, 1985), there are the following modelling guiding principles: (i) dimensional consistency, (ii) coordinate system independence, (iii) Galilean invariance, (iv) realizability, (v) linearity and independence of conserved passive scalars and (vi) boundedness of composition. Apparently, the MSIEM model satisfies the first three principles. Realizability is ensured by the fact that the Lagrangian mixing frequency G_α is positive definite and bounded, provided that G is evaluated as a bounded, positive definite quantity ($0 \leqslant S_{\alpha 3} \leqslant 1$ by definition).

The fifth principle states that arbitrary (non-singular) linear combinations of non-reacting scalars with equal molecular diffusivities should mix according to the same model. The MSIEM model satisfies that constraint provided that all the scalars have the same mixing properties, i.e., if G_α is the same for each scalar. However, in general, the MSIEM model calculates the mixing specifically for each scalar (in dependence on its mean gradients, initial and boundary conditions), such that the fifth

modelling guiding principle is not always satisfied. But, for the set of scalars considered, it is ensured that the scalars evolve independently: Eqs. (5b)–(5c) and (1c) depend for a non-reacting scalar only upon a single scalar subscript (α).

The sixth principle states that at any time, all physical bounds of the scalars should be respected. It is satisfied if the modelled mixing process at any time only generates new states inside the convex region in the sample space which is already occupied by the scalars. As a consequence of considering G_α to be specific for each scalar, the latter property is not always ensured. However, the MSIEM model satisfies the boundedness constraint in its weak formulation: if the initial and boundary values of Φ_α lie within a given range $\Phi_{\alpha,\min} \leqslant \Phi_\alpha \leqslant \Phi_{\alpha,\max}$, then $\Phi_\alpha(\mathbf{x},t)$ for all $(\mathbf{x},t)$ also lies in this range. The latter property limits the possible deviations from the ideal behaviour of a mixing model.

3.3. Algebraic multi-scale Lagrangian mixing model

For applications, an algebraic expression for the mixing frequency G_α is of special interest in order to reduce the computational effort. Such a model is obtained by neglecting in Eqs. (5b)–(5c) the terms on the left-hand side. First, it is worth emphasizing that the neglect of changes of $S_{\alpha 3}$ and $S_{\alpha 2}$ in time and space represents a much weaker assumption than to neglect changes of $\sigma^2_{\alpha 1}$, $\sigma^2_{\alpha 2}$ and $\sigma^2_{\alpha 3}$: only the changes of their ratios to the total composition variance are assumed to be small compared to the other contributions in their transport equations. An algebraic approximation for G_α corresponds to the consideration of the mixing frequency G_α as a property of the flow field: the effects of initial and boundary conditions of $S_{\alpha 2}$ and $S_{\alpha 3}$ on the mixing are neglected, i.e., the mixing frequency is assumed to be controlled by the diffusive flow motion. The neglect of the effects of the $S_{\alpha 2^-}$ and $S_{\alpha 3^-}$ initial conditions is justified for the consideration of mixing for times much longer than the initial stage of mixing, i.e., at least for all statistically stationary flows. The neglect of the dependence of G_α on the boundary values of $S_{\alpha 2}$ and $S_{\alpha 3}$ can be expected to be a valid approximation if the scalar distribution near walls does not cause significant effects, e.g., on mixing and reaction within reaction zones.

To see the relevant effects most clearly, we introduce dimensionless variables: the scalar production-to-dissipation ratio $p_\alpha = \gamma_\alpha/(GS_{\alpha 3})$, and the TKE-to-scalar dissipation time scale ratio $R_\alpha = \tau/\tau_\alpha$, where $\tau_\alpha = (GS_{\alpha 3})^{-1}$. By neglecting the left-hand sides in Eqs. (5b)–(5c) and replacing $S_{\alpha 2}$ in Eq. (5b) through a function of $S_{\alpha 3}$ according to Eq. (5c), the following equation for R_α can be obtained:

$$0 = R_\alpha^3 - \frac{A_1}{1-p_\alpha}R_\alpha^2 + \frac{A_2}{(1-p_\alpha)^2}R_\alpha - \frac{A_3}{(1-p_\alpha)^2}, \qquad (12)$$

where $A_1 = E\tau + G\tau + C_\varphi$, $A_2 = EG\tau^2 + C_\varphi E\tau + C_\varphi G\tau$ and $A_3 = C_\varphi EG\tau^2$. Eq. (12) is solved by ($k = 0, 1, 2$)

$$R_\alpha = \frac{A_1}{3(1-p_\alpha)} + \frac{2}{3}\frac{\sqrt{A_1^2 - 3A_2}}{|1-p_\alpha|}\cos\left\{\frac{\varphi + 2k\pi}{3}\right\}, \qquad (13)$$

where $\varphi = \mathrm{Arccos}\{[A_1^3 - 4.5A_1A_2 + 13.5A_3(1-p_\alpha)](A_1^2 - 3A_2)^{-1/2}|1-p_\alpha|(1-p_\alpha)^{-3}\}$.

Relation (13) permits up to three real and positive solutions, such that the question appears which of these solutions will be realized by the general Eqs. (5b)–(5c). It will be shown in the next section that the minimum of the real and positive solutions which are provided by Eq. (13) will be realized if there is no scalar production, i.e., $p_\alpha = 0$. By extending that analysis, it can be shown numerically (for all initial values $0 \leqslant (S_{\alpha 2}, S_{\alpha 3}) \leqslant 1$) that the same behaviour is found for a non-vanishing p_α. Hence, the algebraic solution of Eqs. (5b)–(5c) is given through the minimum of all real and positive solutions which are provided by Eq. (13). We denote that model as algebraic multi-scale interaction by exchange with the mean (AMSIEM) model.

3.4. Homogeneous, decaying and local equilibrium turbulence

To assess the behaviour of the AMSIEM model, we consider it for two important cases: homogeneous, decaying ($p_\alpha = 0$) and local equilibrium turbulence ($p_\alpha = 1$).

To investigate the first case of homogeneous, decaying turbulence, we neglect all the spatial gradients in Eqs. (5b)–(5c) including γ_α. Under these conditions, the nonlinear and coupled Eqs. (5b)–(5c) can be rewritten into linear equations for combinations of $S_{\alpha 2}$ and $S_{\alpha 3}$,

$$\frac{\mathrm{d}}{\mathrm{d}t}\left(\frac{S_{\alpha 2}}{S_{\alpha 3}-1}+1\right)^{-1} = E\left[\left(\frac{C_\varphi}{E\tau}-1\right)\left(\frac{S_{\alpha 2}}{S_{\alpha 3}-1}+1\right)^{-1}+1\right], \qquad (14a)$$

$$\frac{\mathrm{d}}{\mathrm{d}t}(S_{\alpha 3}-1)^{-1} = -G\left[\left(\frac{E}{G}\frac{S_{\alpha 2}}{S_{\alpha 3}-1}+1\right)(S_{\alpha 3}-1)^{-1}+1\right]. \qquad (14b)$$

Eq. (14a) is closed in the function $S_{\alpha 2}/(S_{\alpha 3}-1)+1$, which is very helpful for the calculation of the asymptotic features of the model. Expression $S_{\alpha 2}/(S_{\alpha 3}-1)+1$ may be written as $S_{\alpha 1}/(S_{\alpha 1}+S_{\alpha 2})$, where $S_{\alpha 1} = \sigma^2_{\alpha 1}/\sigma^2_\alpha$. This shows that $S_{\alpha 2}/(S_{\alpha 3}-1)+1 \geqslant 0$. The coefficient $C_\varphi/(E\tau)-1$ on the right-hand side of Eq. (14a) reveals, that two cases have to be distinguished in order to assess the asymptotic features of the model: $C_\varphi/(E\tau) \geqslant 1$ and $C_\varphi/(E\tau) \leqslant 1$. For $C_\varphi/(E\tau) \geqslant 1$, we find the derivative of

$[S_{\alpha 2}/(S_{\alpha 3}-1)+1]^{-1}$ to be always positive. Thus, $[S_{\alpha 2}/(S_{\alpha 3}-1)+1]^{-1}\to\infty$, that means $S_{\alpha 2}/(S_{\alpha 3}-1)\to -1$ for $t\to\infty$. For $C_\varphi/(E\tau)\leqslant 1$, the function $[S_{\alpha 2}/(S_{\alpha 3}-1)+1]^{-1}$ will grow (decrease) for an initially positive (negative) derivative, till both the terms on the right-hand side balance each other. Hence, we find $S_{\alpha 2}/(S_{\alpha 3}-1)\to -C_\varphi/(E\tau)$ in that case.

With reference to Eq. (14b), we observe that the derivative of $(S_{\alpha 3}-1)^{-1}$ is negative if $(E/G)S_{\alpha 2}/(S_{\alpha 3}-1)+1\leqslant 0$ (we note that $S_{\alpha 3}-1\leqslant 0$). In that case, we find $(S_{\alpha 3}-1)^{-1}\to -\infty$ asymptotically, that means $S_{\alpha 3}\to 1$. For $(E/G)S_{\alpha 2}/(S_{\alpha 3}-1)+1\geqslant 0$, the function $(S_{\alpha 3}-1)^{-1}$ will grow (decrease) for an initially positive (negative) derivative, till the terms on the right-hand side of Eq. (14b) balance each other. Thus, we find $S_{\alpha 3}\to -(E/G)S_{\alpha 2}/(S_{\alpha 3}-1)$ in that case. By adopting the asymptotic values of $S_{\alpha 2}/(S_{\alpha 3}-1)$, -1 and $-C_\varphi/(E\tau)$ for $C_\varphi/(E\tau)\geqslant 1$ and $C_\varphi/(E\tau)\leqslant 1$, respectively, these results are summarized by

$$S_{\alpha 3}=1\begin{cases}\text{for}\quad \dfrac{C_\varphi}{E\tau}\geqslant 1\quad\text{and}\quad \dfrac{E}{G}\geqslant 1\\ \text{or}\quad \dfrac{C_\varphi}{E\tau}\leqslant 1\quad\text{and}\quad \dfrac{C_\varphi}{G\tau}\geqslant 1\end{cases}$$

$$S_{\alpha 3}=\begin{cases}\dfrac{E}{G}\quad\text{for}\quad \dfrac{C_\varphi}{E\tau}\geqslant 1\quad\text{and}\quad \dfrac{E}{G}\leqslant 1\\ \dfrac{C_\varphi}{G\tau}\quad\text{for}\quad \dfrac{C_\varphi}{E\tau}\leqslant 1\quad\text{and}\quad \dfrac{C_\varphi}{G\tau}\leqslant 1\end{cases},\qquad (15)$$

which leads (independent of the chosen initial values for $S_{\alpha 2}$ and $S_{\alpha 3}$) after multiplication with $G\tau$ to the asymptotic (normalized) mixing frequency

$$R_\alpha=\mathrm{Min}(G\tau,E\tau,C_\varphi).\qquad (16)$$

That is a plausible result: the turbulence only dissipates if there is no production, i.e., the mixing intensity R_α will become minimal asymptotically. The value of R_α becomes controlled by the slowest step.

For the second case of local equilibrium turbulence ($p_\alpha=1$) we obtain

$$R_\alpha^{-1}=C_\varphi^{-1}+(E\tau)^{-1}+(G\tau)^{-1}.\qquad (17)$$

That relation simply states that under local equilibrium conditions the characteristic (normalized) mixing time R_α^{-1} is given through the sum of characteristic mixing times of the three considered stages of the scalar spectrum.

By involving the definitions $E=0.058/\tau_\eta$ and $G=(0.303+17050/Sc)E$, R_α is determined through Eq. (13) as a function of Re_1, Sc and p_α. Fig. 2 illustrates these dependencies for a range of (high) Sc und p_α. Findings (16) and (17) are presented in Fig. 2a and c, respectively. These curves quantify our expectation: For growing turbulent Reynolds numbers Re_1, the mixing frequency R_α approaches C_φ asymptotically. An increase of the scalar production-to-dissipation ratio p_α may be seen as an increased production with reference to a (fixed) dissipation, which causes a higher value of $\sigma_{\alpha 1}^2$, see Eq. (4a). For unaffected $\sigma_{\alpha 2}^2$ and $\sigma_{\alpha 3}^2$, $S_{\alpha 3}=\sigma_{\alpha 3}^2/(\sigma_{\alpha 1}^2+\sigma_{\alpha 2}^2+\sigma_{\alpha 3}^2)$ has to decrease. Due to the increased total variance, the characteristic scalar dissipation time $\tau_\alpha=(GS_{\alpha 3})^{-1}$ becomes larger, that means the TKE-to-scalar dissipation time scale ratio $R_\alpha=\tau/\tau_\alpha$ has to decrease for growing p_α. Corresponding findings for gas-phase mixing were reported by Sirivat and Warhaft (1983). The effect of the Schmidt number Sc is consistent with Fig. 1: higher values of Sc increase the characteristic mixing time R_α^{-1}.

4. Application to mixing and parallel chemical reactions in a pipe

The MSIEM model represents a Lagrangian stochastic model that satisfies exactly the transport equations of Baldyga, which are tested for different flows (Baldyga, 1994; Baldyga & Henczka, 1995, 1997; Kruis & Falk, 1996; Baldyga & Bourne, 1999). This fact provides evidence for its good performance. We illustrate this performance here for the pipe flow experiments of Baldyga and Henczka (1997) for two reasons: first, to demonstrate the applicability of the algebraic version AMSIEM of the MSIEM model, and second, to show the remarkable effect of the consideration of mixing processes at the Kolmogorov and Batchelor scale. The simulations of the pipe flow and the mixing and parallel chemical reactions are described in Sections 4.1 and 4.2. The results are summarized in Section 4.3.

4.1. Pipe flow simulation

Experimental investigations were carried out in a tubular reactor with an inner diameter of $D=32$ mm equipped with a concentrically located tube with an inner diameter of 1.81 mm and an outer diameter of 2.52 mm, see Fig. 3. The mean pipe velocity $\langle U_1\rangle$ varied from 0.469 to 2.19 m s^{-1}, which corresponds to a change of the pipe Reynolds number $Re=\langle U_1\rangle D/\nu$ from 15000 to 70000, where the kinematic viscosity $\nu=10^{-6}$ m^2 s^{-1} (Baldyga & Henczka, 1997).

To describe this pipe flow, the Lagrangian equation (1a)–(1c) have to be closed by models for the turbulence time scale τ and the Kolmogorov time scale τ_η, which are required to estimate the frequencies C_φ/τ, E and G. The Schmidt number Sc, which appears in G, is taken to be $Sc=800$. Transport equations for τ in conjunction with Lagrangian flow models were presented for different flows (Pope & Chen, 1990; Dreeben & Pope, 1997b; Heinz, 1998). However, pipe flow simulations in that way were not performed previously. The experience obtained

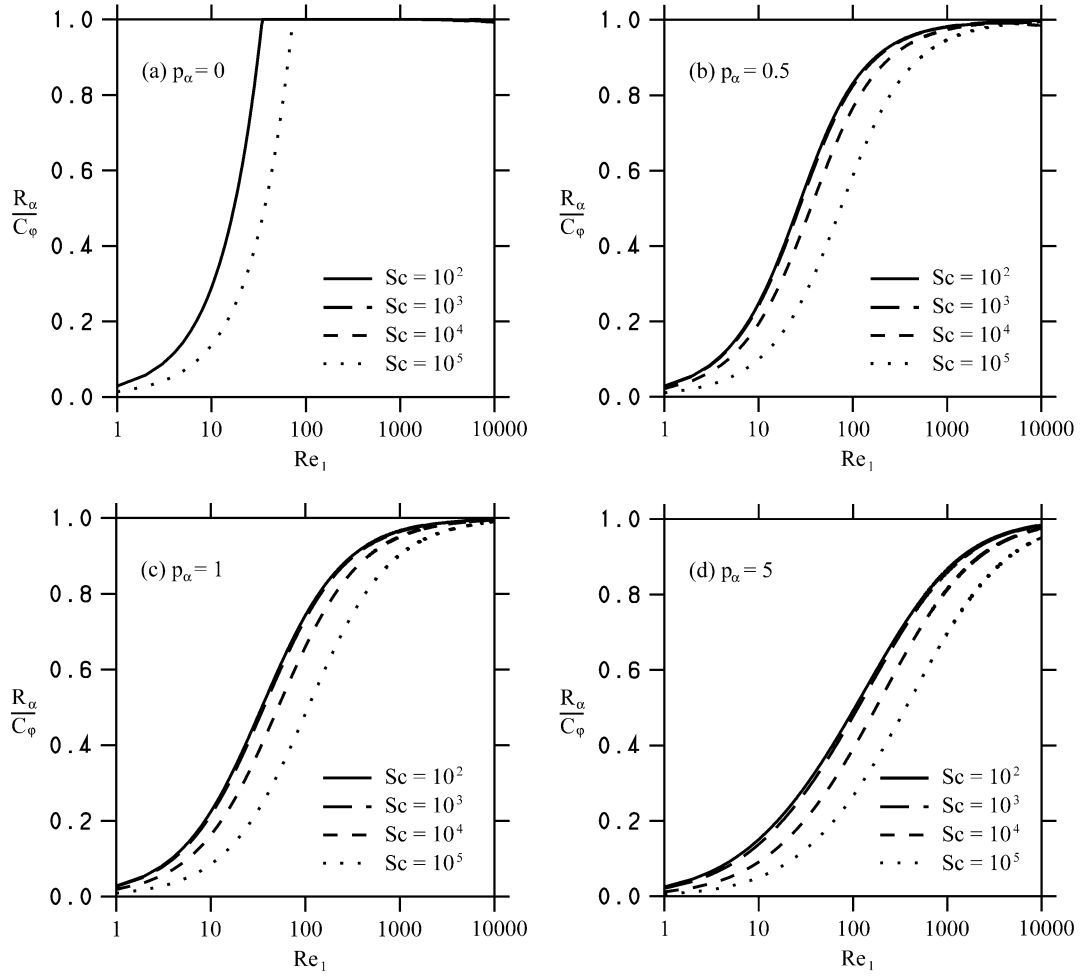

Fig. 2. The normalized composition mixing frequency R_α in dependence on Re_1 for different Sc and p_α, where $C_\varphi = 2.0$. In Fig. 2a, the curves for $Sc = 10^2, 10^3$ and 10^4 coincide.

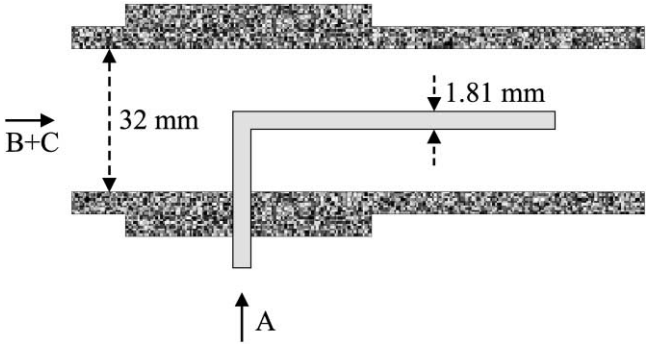

Fig. 3. Illustration of the pipe flow geometry and feed streams A, B and C.

through channel flow simulations led to the conclusion that standard methods have to be extended by the consideration of additional terms (Dreeben & Pope, 1997b). Here our primary interest is in the mixing of species in the reaction zone. In the conditions that will be calculated there is a negligible influence of mean velocity gradients in that zone (Baldyga & Henczka, 1997). Therefore, we derive τ and τ_η from the TKE, which is provided by the Lagrangian equations (1a)–(1b), through an algebraic relation. This approach is advantageous to look at the impact of the variations with Re considered below, because the ratio of these time scales $Re_1 = \tau/\tau_\eta$ is found as a robust function of the TKE. Correspondingly, we apply $\tau = C_\tau D(q^2/2)^{-1/2}$. In that way, τ is calculated as the ratio of the length scale $C_\tau D$ to the characteristic turbulence velocity $(q^2/2)^{1/2}$. The good performance of this model for mixing simulations was tested by Tsai and Fox (1994). C_τ is an open parameter, which may be expected to have a value between 0.057, which arises from the ratio of the two pipe diameters, and 1. We found that the value $C_\tau = C_\mu = 0.09$ brings the best agreement between our flow field simulations, measurements and DNS (Eggels, 1994; Eggels et al., 1994; Toonder & Nieuwstadt, 1997). By calculating the dissipation rate of TKE according to $\varepsilon = q^2/(2\tau)$, the model $\tau = C_\tau D(q^2/2)^{-1/2}$ implies a similar simple expression for the Kolmogorov time scale $\tau_\eta = (C_\tau D\nu)^{1/2}(q^2/2)^{-3/4}$.

Further, boundary conditions for particle velocities have to be provided. As mentioned in Section 2, no attempt is made to include viscous transport in the Lagrangian velocity equation, that means to calculate the wall behaviour explicitly (Dreeben & Pope, 1997a, 1998), because our primary interest is in the study of Reynolds number effects on mixing and reaction. The effect of the pipe wall is taken into account here by adopting boundary conditions which reflect the wall influence (Dreeben & Pope, 1997b). This corresponds with the application of wall-functions in Reynolds-stress closure models. The purpose of this approach is to avoid the computational expense which is required to resolve the steep gradients of statistics that appear in the viscous sublayer, while nevertheless correctly represents the well-known near-wall features. These characteristic features of the wall layer have been found to be reasonably robust for flows in channels, pipes, and boundary layers: In the inertial sublayer, the profile of mean velocity is a logarithmic function of the wall-normal distance, the dissipation varies inversely with that distance, and the production and dissipation of TKE are approximately equal to one another (Dreeben & Pope, 1997b).

According to the approach of Dreeben and Pope (1997b), the following boundary conditions are applied to the streamwise (U_1^*) and radial (U_r^*) particle velocities: $U^*_{r(R)} = -U^*_{r(I)}$ and $U^*_{1(R)} = U^*_{1(I)} + \alpha U^*_{r(I)}$, where the subscripts I and R denote the values before and after reflection, respectively. The coefficient α determines the correlation coefficient at the reflection plane, $\alpha = -2\langle u_1 u_r\rangle/\langle u_r^2\rangle$. In accord with pipe measurements and DNS (Eggels, 1994; Eggels et al., 1994; Toonder & Nieuwstadt, 1997), we applied $\alpha = 0$ at the centreline, and at the outer pipe radius we used $\alpha = 1$.

The simulations were carried out by means of the code PDF2DV (Pope, 1994b). Only the domain between symmetry axis and wall is considered. The domain is discretized into (radial) 18 and (streamwise axial) 75 cells. The radial extent of the source corresponds to the radius of the first grid cell. A non-uniform grid spacing was applied in the streamwise direction, so that the ratio between the length of the first cell (at the inlet) to that of the last cell was 1/5. With that spacing, the length of the first cell was approximately of the same size as the radial cell length. It was proved that a higher spatial resolution (a ratio of 1/10 between the lengths of the first and last cells in the streamwise direction and 50% more grid points) had no influence on the results. The extent of the computational domain was $10D$ in the streamwise direction. The mean particle streamwise velocity at the inlet region was derived from the Reynolds number by $\langle U_1\rangle = Rev/D$, and the radial mean particle velocity was set to zero. For the turbulence intensity we applied, independent of Re, 0.16 at the inlet region (Eggels, 1994; Eggels et al., 1994; Toonder & Nieuwstadt, 1997). The influence of variations of 50% of this value on the results presented in Section 4.3 is lower than 0.2%. The initial values for τ and τ_η were chosen according to their relation with the TKE. The latter results from the specified $\langle U_1\rangle$ and the turbulence intensity.

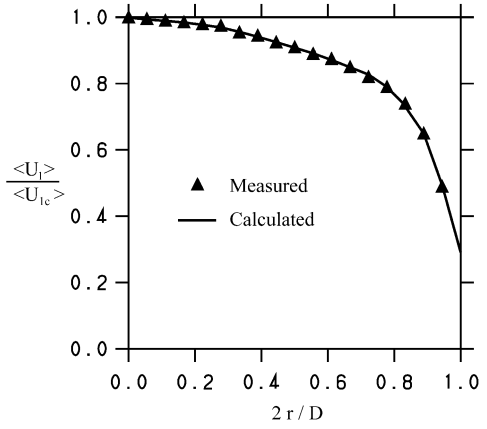

Fig. 4. Mean axial velocity $\langle U_1\rangle$ normalized on the centreline velocity $\langle U_{1c}\rangle$ as function of the normalized radial distance $2r/D$ from the centreline. D is the pipe diameter and r the radial coordinate. The triangles represent laser-Doppler anemometry (LDA) measurements, which agree very well with hot-wire anemometry (HWA) and particle image velocimetry (PIV) measurements and DNS data (Eggels, 1994; Eggels et al., 1994).

The radial profile of the mean streamwise velocity obtained with these initial and boundary conditions is compared to the results of measurements in Fig. 4. This figure shows the correct simulation of the velocity field. It was proved that the other flow field quantities were obtained in accord with the features found in measurements and DNS (Eggels, 1994; Eggels et al., 1994; Toonder & Nieuwstadt, 1997). A detailed description of the performance of the same code for similar conditions can be found elsewhere (Dreeben & Pope, 1997b).

4.2. Simulation of mixing and parallel chemical reactions

The experimental investigations of the mixing and reaction of species were carried out by introducing a premixture of hydrochloric acid (B = HCl) and ethyl chloroacetate ($C = CH_2ClCOOC_2H_5$) over the reactor cross-sectional area. A solution of sodium hydroxide (A = NaOH) was fed through the concentrically located injector, see Fig. 3. These species react according to

$$A + B \xrightarrow{k_1} P_1, \quad A + C \xrightarrow{k_2} P_2, \tag{18}$$

where $k_1 \to \infty$, $k_2 = 23\ \mathrm{dm^3/(mol\,s)}$ at a temperature $T = 293$ K. P_1 and P_2 are the reaction products. Such parallel chemical reactions were proposed to characterize mixing by Baldyga and Bourne (1990). This reaction scheme represents the structure of many important chemical process engineering or environmental applications

(Fox, 1996; Baldyga & Bourne, 1999). As shown below, the efficiency of chemical conversions according to Eq. (18) may depend very sensitively on mixing. This quantity can be evaluated through the final selectivity X_s of forming P_2, which is proportional to the decrease of the C-concentration along the reactor

$$X_s = \frac{\bar{C}_{C_0} - \bar{C}_{C,out}}{\bar{C}_{A_0}}, \tag{19}$$

where $\bar{C}_{C_0}$, $\bar{C}_{A_0}$ and $\bar{C}_{C,out}$ are the inlet concentrations of C and A and the outlet concentration of C, respectively, averaged over the reactor diameter. These quantities were measured chromatographically (Baldyga & Henczka, 1997).

The calculation of the reaction between A, B and C requires an appropriate handling of the infinitely fast reaction between A and B. These species cannot coexist, i.e., the consideration of their difference is sufficient. Therefore, instead of C_A, C_B and C_C we consider only two dimensionless concentration differences:

$$\Phi_Z = \frac{C_A - C_B}{C_{A_0}}, \tag{20a}$$

$$\Phi_f = \frac{C_A - C_B - C_C + C_{B_0} + C_{C_0}}{C_{A_0} + C_{B_0} + C_{C_0}}, \tag{20b}$$

where C_{A_0}, C_{B_0} and C_{C_0} are the initial concentrations of A, B and C. Relation (18) reveals that the reaction rate of Φ_f is zero. The reaction rate $\rho^{-1} r_Z$ of Φ_Z is zero for negative Φ_Z and otherwise given by

$$\rho^{-1} r_Z = -k_2 C_{A_0} \Phi_Z (\Phi_Z - \Phi_Z^{\infty}). \tag{21}$$

In Eq. (21), $\Phi_Z^{\infty} = \Phi_f (C_{A_0} + C_{B_0} + C_{C_0})/C_{A_0} - (C_{B_0} + C_{C_0})/C_{A_0}$ is used, which is Φ_Z for $k_2 = k_1 \to \infty$. The consideration of Φ_f and Φ_Z is sufficient for the calculation of X_s, because the concentration C_C is determined by these quantities,

$$C_C = C_{A_0} (\Phi_Z - \Phi_Z^{\infty}). \tag{22}$$

Calculations of X_s according to Eq. (19) were performed for Re-variations between 15000 and 70000 and various initial concentrations for A, B and C: (a) $C_{A_0} = 0.45$ mol/dm^3, $C_{B_0} = C_{C_0} = 0.009$ mol/dm^3, (b) $C_{A_0} = 0.9$ mol/dm^3, $C_{B_0} = C_{C_0} = 0.018$ mol/dm^3, (c) $C_{A_0} = 0.45$ mol/dm^3, $C_{B_0} = C_{C_0} = 0.014$ mol/dm^3. The mixing of Φ_f and Φ_Z was calculated by the AMSIEM (13), where the expression $\gamma_\alpha = \lambda\tau(q^2/\sigma_\alpha^2)\,[\partial\langle C_\alpha\rangle/\partial x_j]^2$ was applied to estimate γ_α.

4.3. Results

The results of the simulations described in Sections 4.1 and 4.2 are presented in Fig. 5. The fact that in this experiment the selectivity X_s depends on the Reynolds number Re can be explained as follows. Close to the injector, there is a lot of A compared to B + C. After consumption of part of A by the reaction with B there remains A to participate in the second reaction. The higher $Re = \langle U_1\rangle D/\nu$ (or the inlet flow velocity, respectively), the smaller is the selectivity X_s due to the slower chemistry between A and C. This dependence of the chemistry on the Reynolds number can be made explicit by means of the Damköhler number $Da_C = 2k_2 \bar{C}_A \tau/R_C$ (R_C is written for R_α here) for the reaction between A and C. By means of $\tau = C_\tau D(q^2/2)^{-1/2}$ and $\langle U_1\rangle = Re\nu/D$ we find $Da_C = 2k_2\ \bar{C}_A\ C_\mu D^2/(i\nu Re R_C)$, where $i = (q^2/2)^{1/2}/\langle U_1\rangle$ is proportional to the turbulence intensity. This quantity is independent of Re (Eggels, 1994; Eggels et al., 1994; Toonder & Nieuwstadt, 1997), so that Da_C is found to be inversely proportional to $\nu Re R_C$ (R_C grows with increasing Re, see Fig. 6). The effect of Da_C can also be observed by comparing Figs. 5a and 5b. Due to the chosen initial concentration of A, the Damköhler number Da_C related to Fig. 5b is twice the value of Da_C related to Fig. 5a. At $Re = 15\,000$, the inlet values of these Damköhler numbers are $Da_C = 0.38$ and 0.19, respectively.

The comparison with the measurements reveals the good performance of the AMSIEM model: all calculated results are within the range of accuracy (± 0.007 practically independent of Re (Baldyga, 1999)) of the experimental data. The neglect of Re-effects, i.e., the calculation of the mixing with the usually applied mixing rate C_φ/τ instead of R_α/τ, leads to a remarkable underestimate of the selectivity X_s, which amounts to approximately 50% for $Re = 15\,000$. The reason for this difference is given by the fact that C_φ/τ provides a too strong mixing between A and B + C. In that case, X_s decreases due to the infinitely fast destruction of A through reaction with B, i.e., there is less A left to participate in the reaction with C. The overprediction of mixing through C_φ/τ is illustrated in Fig. 6, where $E\tau/C_\varphi = 0.029\,Re_1$ and R_α/C_φ are shown along the centreline for $Re = 15\,000$ and $70\,000$. The normalized composition frequency of the model that applies C_φ/τ as mixing rate is given by 1. The values of $E\tau/C_\varphi$ indicate for the different Reynolds numbers the relevance of Re-effects and demonstrate the applicability of Baldyga's approach because $Re_1 \geqslant 11.6$. For $\gamma_\alpha = 0$, the calculated mixing frequency R_α/τ would be equal to E, but the appearance of a streamwise scalar gradient in conjunction with small values for the variance of Φ_f results in values of $\gamma_\alpha\ \tau/C_\varphi$ near 0.5 in the reaction zone, which leads to a smaller mixing frequency R_α/τ.

5. Summary

We presented a new Lagrangian mixing model that simulates in accord with Eulerian transport equations for means and variances the turbulent mixing of reacting scalars as a cascade process from large to small scales. In contrast to the description of these processes in the

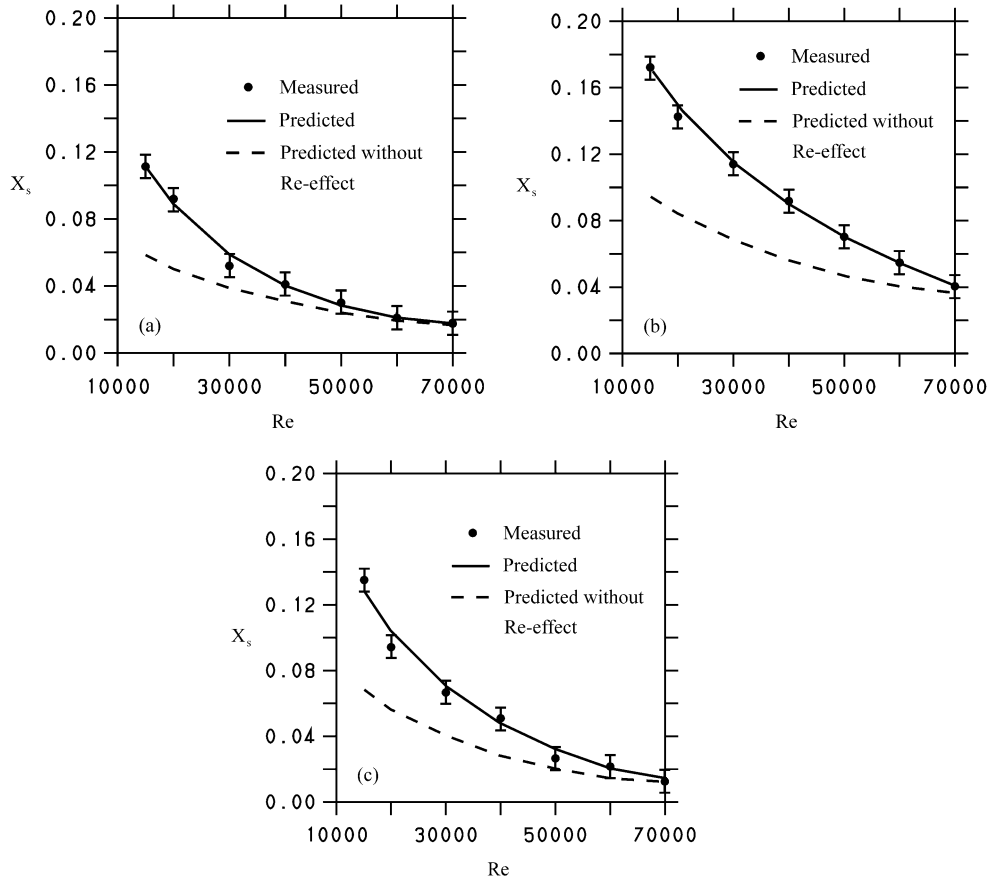

Fig. 5. Product distribution X_s vs. Reynolds number Re. The initial feed concentrations of A, B and C are: (a) $C_{A_o} = 0.45\,\mathrm{mol/dm^3}$, $C_{B_o} = C_{C_o} = 0.009\,\mathrm{mol/dm^3}$, (b) $C_{A_o} = 0.9\,\mathrm{mol/dm^3}$, $C_{B_o} = C_{C_o} = 0.018\,\mathrm{mol/dm^3}$, (c) $C_{A_o} = 0.45\,\mathrm{mol/dm^3}, C_{B_o} = C_{C_o} = 0.014\,\mathrm{mol/dm^3}$. The dashed line gives the result of the model that applies C_φ/τ as mixing rate. The error bars denote the accuracy of these measurements.

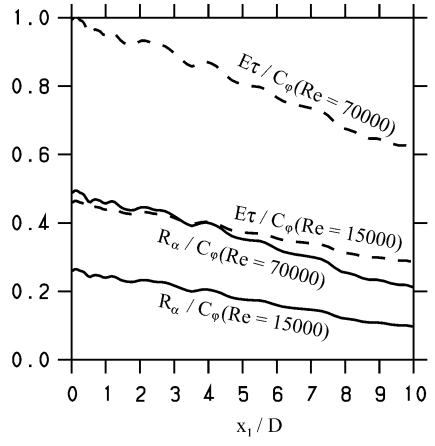

Fig. 6. The normalized composition mixing frequency R_α/C_φ and $E\tau/C_\varphi$ along the pipe centreline for $Re = 15\,000$ and $70\,000$.

Eulerian framework, no closure assumptions on mean reaction rates are required in the Lagrangian approach applied here, i.e., approximations are restricted to the simulation of mixing processes. In contrast to previously applied methods in the Lagrangian approach, the derived mixing model is shown to be applicable to the calculation of the multi-scale turbulent mixing in inhomogeneous liquid-phase reacting flows. This is of relevance to both chemical engineering applications and the further development of models that describe multi-scale mixing in multi-phase flows.

Two new findings are presented here, which are of interest from a theoretical point of view: First, it has been demonstrated that scalar gradients (the scalar production-to-dissipation ratio) may lead to a significant reduction of the composition frequency. Second, it has been shown that simple algebraic models for the composition frequency, which are of special relevance to the evaluation of complex turbulence-chemistry interactions, can be derived by means of relatively weak assumptions, see Section 3.3. The methodology used here to construct the mixing model can be applied in consistency with other Eulerian variance transport equations and other Lagrangian (frame) models than the simple models used here to illustrate the approach. Additionally, the presented description of micromixing can be adopted in computationally less-demanding PDF methods as the multi-environment CFD micromixing model (Fox, 1998).

The MSIEM model can be seen as proved for different flows through its full consistency with the well-tested transport equations of Baldyga. The good performance of its algebraic version, i.e., of the AMSIEM model, was illustrated in Section 4. It was shown that in the simulations of the tubular reactor experiments of Baldyga and Henczka (1997) the inclusion of Reynolds number effects leads to good results in contrast with the use of the standard mixing frequency of the large-scale turbulence that results in errors up to 50%. The errors of calculations where mixing at the Kolmogorov and Batchelor scale is not accounted for may be much larger, if more complex reaction mechanisms have to be considered.

Notation

A_1, A_2, A_3 parameters in the AMSIEM model
A, B, C species involved in the reactor chemistry
C_0 parameter in the Lagrangian velocity equation (= 3.5)
C_φ parameter in the Lagrangian species equation (= 2.0)
C_τ parameter in the τ-equation ($= C_\mu = 0.09$)
C_α concentration of species α
$C_{A_0}, C_{B_0}, C_{C_0}$ initial species concentrations

$C_{C,out}$ outlet concentration of C
D reactor diameter
D_m, D_T molecular and turbulent diffusivities
Da_C Damköhler number ($= 2k_2 \bar{C}_A \tau / R_C$)
E characteristic frequency in the multiscale model ($= 0.058/\tau_\eta$)
E_u, E_Φ velocity and scalar spectral density functions
G characteristic frequency in the multiscale model ($= (0.303 + 17\,050/Sc)E$)
G_α mixing frequency in the Lagrangian species equation ($= Re_\alpha/(2\tau)$)
P_1, P_2 reaction products
Re Reynolds number ($= \langle U_1 \rangle D/\nu$)
Re_1 turbulent Reynolds number ($= \tau/\tau_\eta$)
Re_λ Taylor-scale Reynolds number ($= 2.582\ Re_1$)
R_α TKE-to-scalar dissipation time scale ratio ($= \tau/\tau_\alpha$)
R_C R_α for the substance C
Sc Schmidt number ($= \nu/D_m$)
$S_{\alpha i}$ $i = 1, 2, 3$ $= (\sigma_{\alpha i}^2/\sigma_\alpha^2$ where $i = 1, 2, 3)$
T temperature
U_i^* ith component of the Lagrangian velocity
U_r^* radial Lagrangian velocity component
U_i ith component of the Eulerian velocity
W_i ith component of a Wiener vector process
X_s selectivity of forming the reaction product P_2
c_α Eulerian concentration fluctuation
i ($= (q^2/2)^{1/2}/\langle U_1 \rangle$)
k wavenumber
k_0 peak wavenumber of the energy spectrum
k_K Kolmogorov-scale wavenumber
k_B Batchelor-scale wavenumber
k_1, k_2 reaction constants
p mean pressure
p_α scalar production-to-dissipation ratio ($= \gamma_\alpha/(GS_{\alpha 3})$)
q^2 twice the TKE ($= \langle u_i u_i \rangle$)
r radial distance from the reactor centreline
r_α chemical source term in the Lagrangian concentration equation
t time
u_i ith component of the Eulerian velocity fluctuation
u_r radial component of the Eulerian velocity fluctuation
x_i^* ith component of the particle position
x_i ith component of the position vector

Greek letters

α ($= -2\langle u_1 u_r \rangle / \langle u_r^2 \rangle$)
δ_{ij} Kronecker symbol
$\delta(\tau)$ delta function
ε mean dissipation rate of TKE
γ_α scalar gradient term in the MSIEM model
λ ($= 8C_0/[(3C_0 + 2)(3C_0 + 2 + 4G_\alpha\ \tau)]$)
ν kinematic viscosity
ρ mean fluid density
σ_α^2 scalar variance ($= \langle c_\alpha^2 \rangle$)
$\sigma_{\alpha i}^2$ ith spectral contribution to $\sigma_\alpha^2 = \sigma_{\alpha 1}^2 + \sigma_{\alpha 2}^2 + \sigma_{\alpha 3}^2$
τ time scale of TKE dissipation ($= q^2/(2\varepsilon)$)
τ_η Kolmogorov time scale ($= (\nu/\varepsilon)^{1/2}$)
τ_α scalar time scale ($= (GS_{\alpha 3})^{-1}$)
φ parameter in the AMSIEM model
Φ_α^* Lagrangian mass fraction of the scalar α
Φ_α Eulerian mass fraction of the scalar α
Φ_f dimensionless concentration difference
Φ_Z dimensionless concentration difference
Φ_Z^∞ Φ_Z for $k_2 = k_1 \to \infty$

Symbols

$\langle Q \rangle$ Reynolds-averaged variable Q
$\bar{Q}$ Q averaged over the reactor diameter

Acknowledgements

We thank Dr. G. Colenbrander (Shell Amsterdam) for stimulating our interest in the Lagrangian PDF simulation of the reactor chemistry. We would like to especially

thank Professor J. Baldyga (Warsaw University of Technology) for his kind support of our work. He gave us many important hints to the features of his Eulerian multi-scale turbulent mixer model in comparison to other approaches, and he provided us detailed information about the measurements used here to illustrate the performance of our model. Many thanks are also to Professor S. B. Pope for his advice and for allowing access to his PDF2DV code. We gratefully acknowledge the Delft Centre for High Performance Applied Computing for a generous amount of computing time. We are thankful to the referees for their helpful comments.

References

Baldyga, J. (1989). Turbulent mixer model with application to homogeneous, instantaneous chemical reactions. *Chemical Engineering Science*, *44*, 1175–1182.

Baldyga, J. (1994). A closure model for homogeneous chemical reactions. *Chemical Engineering Science*, *49*, 1985–2003.

Baldyga, J. (1999). Personal communication.

Baldyga, J., & Bourne, J. R. (1984a). A fluid mechanical approach to turbulent mixing and chemical reactions. Part I. Inadequacies of available methods. *Chemical Engineering Communications*, *28*, 231–241.

Baldyga, J., & Bourne, J. R. (1984b). A fluid mechanical approach to turbulent mixing and chemical reactions. Part II. Micromixing in the light of turbulence theory. *Chemical Engineering Communications*, *28*, 243–258.

Baldyga, J., & Bourne, J. R. (1984c). A fluid mechanical approach to turbulent mixing and chemical reactions. Part III. Computational and experimental results for the new micromixing model. *Chemical Engineering Communications*, *28*, 259–281.

Baldyga, J., & Bourne, J. R. (1988). Micromixing in inhomogeneous turbulence. *Chemical Engineering Science*, *43*, 107–112.

Baldyga, J., & Bourne, J. R. (1989). Simplification of micromixing calculations. I. Derivation and application of new model. *Chemical Engineering Journal*, *42*, 83–92.

Baldyga, J., & Bourne, J. R. (1990). The effect of micromixing on parallel reactions. *Chemical Engineering Science*, *45*, 907–916.

Baldyga, J., & Bourne, J. R. (1999). *Turbulent mixing and chemical reactions.* Chichester, New York, Weinheim, Brisbane, Singapore, Toronto: Wiley.

Baldyga, J., & Henczka, M. (1995). Closure problem for parallel chemical reactions. *Chemical Engineering Journal*, *58*, 161–173.

Baldyga, J., & Henczka, M. (1997). Turbulent mixing and parallel chemical reactions in a pipe — application of a mixing model. *Récents Progrés en Génie des Procédés*, vol. 11, No. 51 (pp. 341–348). ISBN 2-910239-25-X, Paris, France: Lavoisier.

Chasnov, J. R. (1998). The viscous-convective subrange in nonstationary turbulence. *Physics of Fluids*, *10*, 1191–1205.

Colucci, P. J., Jaberi, F. A., Givi, P., & Pope, S. B. (1998). Filtered density function for large eddy simulations of turbulent reactive flows. *Physics of Fluids*, *10*, 499–515.

Dreeben, T. D., & Pope, S. B. (1997a). Probability density function and reynolds-stress modeling of near-wall turbulent flows. *Physics of Fluids*, *9*, 154–163.

Dreeben, T. D., & Pope, S. B. (1997b). Wall-function treatment in PDF methods for turbulent flows. *Physics of Fluids*, *9*, 2692–2703.

Dreeben, T. D., & Pope, S. B. (1998). Probability density function/Monte Carlo simulation of near-wall turbulent flows. *Journal of Fluid Mechanics*, *357*, 141–166.

Eggels, J. G. M. (1994). *Direct and large eddy simulation of turbulent flow in a cylindric pipe geometry.* Ph.D. thesis, Delft University of Technology, The Netherlands.

Eggels, J. G. M., Unger, F., Weiss, M. H., Westerweel, J., Adrian, R. J., Friedrich, R., & Nieuwstadt, F. T. M. (1994). Fully developed pipe flow: A comparison between direct numerical simulation and experiment. *Journal of Fluid Mechanics*, *268*, 175–209.

Fox, R. O. (1995). The spectral relaxation model of the scalar dissipation rate in homogeneous turbulence. *Physics of Fluids*, *7*, 1082–1094.

Fox, R. O. (1996). Computational methods for turbulent reacting flows in the chemical process industry. *Revue de l'Institut Français du Pétrole*, *51*, 215–243.

Fox, R. O. (1997). The Lagrangian spectral relaxation model of the scalar dissipation rate in homogeneous turbulence. *Physics of Fluids*, *9*, 2364–2386.

Fox, R. O. (1998). On the relationship between Lagrangian micromixing models and computational fluid dynamics. *Chemical Engineering Process*, *37*, 521–535.

Fox, R. O. (1999). The Lagrangian spectral relaxation model for differential diffusion in homogeneous turbulence. *Physics of Fluids*, *11*, 1550–1571.

Gardiner, C. W. (1983). *Handbook of statistical methods.* Berlin, Heidelberg, New York, Tokyo: Springer.

Heinz, S. (1997). Nonlinear Lagrangian equations for turbulent motion and buoyancy in inhomogeneous flows. *Physics of Fluids*, *9*, 703–716.

Heinz, S. (1998). Time scales of stratified turbulent flows and relations between second-order closure parameters and flow numbers. *Physics of Fluids*, *10*, 958–973.

Kolmogorov, A. N. (1942). Equations of turbulent motion of an incompressible fluid. *Izvestiya Academic Nauk SSSR, Series Fizika*, *6*, 56–58.

Kruis, F. E., & Falk, L. (1996). Mixing and reaction in a tubular jet reactor — a comparison of experiments with a model-based on a prescript PDF. *Chemical Engineering Science*, *51*, 2439–2448.

Pope, S. B., & Chen, Y. L. (1990). The velocity-dissipation probability density function model for turbulent flows. *Physics of Fluids*, *A 2*, 1437–1449.

Pope, S. B. (1983). Consistent modelling of scalars in turbulent flows. *Physics of Fluids*, *26*, 404–408.

Pope, S. B. (1985). PDF methods for turbulent reactive flows. *Progress in Energy and Combustion Science*, *11*, 119–192.

Pope, S. B. (1991). Application of the velocity-dissipation probability density function to inhomogeneous turbulent flows. *Physics of Fluids*, *A 3*, 1947–1957.

Pope, S. B. (1994a). On the relationship between stochastic Lagrangian models of turbulence and second-moment closures. *Physics of Fluids*, *6*, 973–985.

Pope, S. B. (1994b). *A Fortran code to solve the modelled joint PDF equations for two-dimensional recirculating flows*. Cornell University, unpublished.

Pope, S. B. (2000). *Turbulent flows*. Cambridge: Cambridge University Press.

Risken, H. (1984). *The Fokker–Planck equation*. Berlin, Heidelberg, New York: Springer.

Rotta, J. C. (1951). Statistische Theorie nichthomogener Turbulenz. *Zeitschrift fuer Physik*, *129*, 547–572.

Sawford, B. L. (1991). Reynolds number effects in Lagrangian stochastic models of turbulent dispersion. *Physics of Fluids*, *A 6*, 1577–1586.

Sirivat, A., & Warhaft, Z. (1983). The effect of a passive cross-stream temperature gradient on the evolution of temperature variance and heat flux in grid turbulence. *Journal of Fluid Mechanics*, *128*, 323–346.

Sreenivasan, K. R. (1996). The passive scalar spectrum and the Obukhov–Corrsin constant. *Physics of Fluids*, *8*, 189–196.

Tennekes, H., & Lumley, J. L. (1972). *A first course in turbulence*. Cambridge, MA: MIT Press.

Toonder, J. M. J., & Nieuwstadt, F. T. M. (1997). Reynolds number effects in a turbulent pipe flow for low to moderate Re. *Physics of Fluids*, *9*, 3398–3409.

Tsai, K., & Fox, R. O. (1994). PDF simulation of a turbulent series-parallel reaction in an axisymmetric reactor. *Chemical Engineering Science*, *49*, 5141–5158.

Tsai, K., & Fox, R. O. (1995). Modeling multiple reactive scalar mixing with the generalized IEM model. *Physics of Fluids*, *7*, 2820–2830.

Van Slooten, P. R., Jayesh, ., & Pope, S. B. (1998). Advances in PDF modeling for inhomogeneous turbulent flows. *Physics of Fluids*, *10*, 246–265.

Wouters, H. A., Peeters, T. W. J., & Roekaerts, D. (1996). On the existence of a generalized Langevin model representation for second-moment closures. *Physics of Fluids*, *8*, 1702–1704.